



## Improved tungsten nanofabrication for hard X-ray zone plates



Karolis Parfeniukas<sup>a,\*</sup>, Jussi Rahomäki<sup>a</sup>, Stylianos Giakoumidis<sup>a</sup>, Frank Seiboth<sup>b</sup>, Felix Wittwer<sup>c</sup>, Christian G. Schroer<sup>c</sup>, Ulrich Vogt<sup>a</sup>

<sup>a</sup> Department of Applied Physics, KTH Royal Institute of Technology, SE-10691 Stockholm, Sweden

<sup>b</sup> Institute of Structural Physics, Technische Universität Dresden, D-01062 Dresden, Germany

<sup>c</sup> Deutsches Elektronen Synchrotron DESY, D-22607 Hamburg, Germany

### ARTICLE INFO

#### Article history:

Received 10 November 2015

Received in revised form 15 December 2015

Accepted 21 December 2015

Available online 22 December 2015

#### Keywords:

X-ray diffractive optics

Zone plate

Tungsten

High aspect ratio

Reactive ion etching

### ABSTRACT

We present an improved nanofabrication method of high aspect ratio tungsten structures for use in high efficiency nanofocusing hard X-ray zone plates. A ZEP 7000 electron beam resist layer used for patterning is cured by a second, much larger electron dose after development. The curing step improves pattern transfer fidelity into a chromium hard mask by reactive ion etching using  $\text{Cl}_2/\text{O}_2$  chemistry. The pattern can then be transferred into an underlying tungsten layer by another reactive ion etching step using  $\text{SF}_6/\text{O}_2$ . A 630 nm-thick tungsten zone plate with smallest line width of 30 nm was fabricated using this method and characterized. At 8.2 keV photon energy the device showed an efficiency of 2.2% with a focal spot size at the diffraction limit, measured at Diamond Light Source I-13-1 beamline.

© 2015 Published by Elsevier B.V.

### 1. Introduction

Hard X-ray nanoimaging using synchrotron radiation is a powerful tool used in a variety of scientific disciplines [1]. In this technique, samples are investigated in a tightly focused X-ray nanobeam produced by advanced X-ray optics. Although the design of latest-generation synchrotron radiation facilities will allow for an increase in coherence and photon flux at the sample [2], current instruments are still limited by the resolution and quality of the focusing optics. Therefore, improvements in the fabrication of X-ray optics are still required to harness the full potential of X-ray nanoimaging.

One important optical device widely used at synchrotron facilities to achieve sub-50 nm hard X-ray focusing is the Fresnel zone plate. It is a circular diffraction grating with radially decreasing linewidth [3]. Two principal quality characteristics of zone plates are considered to be their resolution and first-order diffraction efficiency. The resolution is defined by outermost zone width, while the efficiency peaks at a certain structure height. E.g., to focus 8.2 keV photon energy X-rays with maximum efficiency, a tungsten grating of 1.6  $\mu\text{m}$  thickness is required. Consequently, very high aspect ratio structures are desirable in this kind of optics.

Tungsten has been previously shown to be an attractive zone plate material because small nanostructures for high resolution can be achieved [4], as well as adequate device thickness for high

efficiency [5]. However, these two features have not been demonstrated at the same time. In this paper, we bridge the gap between resolution and efficiency by providing an optimized nanofabrication method of tungsten structures with an aspect ratio of 21:1 at 30 nm line width.

Alternative nanofabrication methods have been developed to manufacture high aspect ratio structures for X-ray diffractive optics. Atomic layer deposition can be used as a zone-doubling technique to achieve aspect ratios of 42:1 with line width of 32 nm [6], 27.5:1 with line width 20 nm [7], and 16:1 with line width of 12.5 nm [8]. Nevertheless, the process only produces structures of uniform width. Other methods can be used to further increase the effective aspect ratio. For example, fabricating two zone plates on both sides of the substrate provides an aspect ratio of 40:1 [9], at the cost of complicated alignment and fabrication procedures. Multilayer Laue lenses can provide virtually unlimited aspect ratio, but are currently limited to an aperture of approx. 40  $\mu\text{m}$  [10], severely reducing the amount of photons in the focus for larger X-ray beam illumination sizes.

In this paper, we present an improvement on the process of tungsten zone plate nanofabrication. We report an enhancement of the pattern transfer quality and effectiveness by employing resist curing with e-beam. This additional step allows for reduction of smallest structure width down to 30 nm while still maintaining relatively large structure height upwards of 600 nm. Overall we were able to improve the aspect ratio to 21:1. The process can be used not only to produce zone plates, but also other important devices for X-ray nanoimaging such as test patterns with very small features.

\* Corresponding author.

E-mail address: [karolisp@kth.se](mailto:karolisp@kth.se) (K. Parfeniukas).

## 2. Materials and methods

### 2.1. Fabrication

Fig. 1 illustrates the fabrication process of tungsten zone plates. It is based on a previously developed method of transferring an electron-beam-defined pattern into a thick tungsten layer. The principal improvement is improving the etch resistance of the electron beam resist layer by exposing it by an electron beam again after development. The entire fabrication process is described in detail below.

As a substrate, a 1  $\mu\text{m}$  thick silicon nitride membrane on a supporting silicon frame is used (Silson Ltd.). Firstly, it is covered with a 5 nm chromium layer by electron beam evaporation at a low base pressure of  $10^{-8}$  mbar in an in-house system (Thermionics/Eurovac). This layer acts as an etch stop during the tungsten etch step.

Then, an approximately 600 nm thick layer of tungsten is sputtered on top of the chromium layer in an AJA Orion system (AJA International). The deposition is performed at the following parameters: 20 sccm argon gas flow, 5 sccm nitrogen gas flow, 10 mTorr pressure, 150 W DC power, and 250  $^{\circ}\text{C}$  temperature. The resulting deposition rate is 11 nm/min. The parameters have been optimized to obtain tungsten films with low internal stress, reducing the grain size and thusly increasing achievable etch resolution in the material [11]. However, it must be noted that introducing nitrogen gas during the sputtering process somewhat decreases the density of the deposited film, and, therefore, slightly reduces the maximum obtainable efficiency of the device.

Afterwards, a 25 nm thick chromium hardmask is deposited by electron beam evaporation, similarly to the etch stop.

Next, an 80 nm film of ZEP 7000 solution (Zeon Chemicals, L.P.) is spin-coated on top of the sample and baked at 170  $^{\circ}\text{C}$  in a convection oven for 30 min.

The electron beam pattern defining the zone plate structures was exposed using a 100 keV electron beam lithography tool (Vistec EBPG5000+) with a dose varying from 610  $\mu\text{C}/\text{cm}^2$  to 1010  $\mu\text{C}/\text{cm}^2$ .

After exposure, the resist was developed for 30 s in  $-18$   $^{\circ}\text{C}$  hexylacetate, then rinsed in isopropanol and pentane, an adaptation from a study presented earlier [12].

Before any pattern transfer is performed, the zone plate area was exposed again at 5 kV and a 30,000  $\mu\text{C}/\text{cm}^2$  dose in a Raith 150 system (Raith GmbH). This extreme dose increases etch resistance in the steps that follow. We believe that the increased resistance is a result of stronger molecule cross-linking in the resist, related to the fact that the tone of the ZEP 7000 resist changes from positive to negative [13, 14]. The curing is what ultimately permitted us to reach 30 nm structure width in the outermost zones of the zone plates. A comparison between cured and non-cured resist performances is depicted in Fig. 2.

The electron beam resist pattern is transferred into the chromium hardmask using reactive ion etching (RIE) in a Plasmalab 100 system (Oxford Instruments). This etch step is performed using  $\text{Cl}_2$  and  $\text{O}_2$  at 8 sccm and 2 sccm gas flow, respectively, 20 mTorr pressure, 11 W RF power, 20 W ICP power, and 30  $^{\circ}\text{C}$  substrate temperature, resulting in an etch rate of 2.5 nm/min.

The chromium mask pattern is then finally transferred into tungsten in the same RIE system. The parameters are as follows:  $\text{SF}_6$  and  $\text{O}_2$  at 8 sccm and 2 sccm gas flow, respectively, 4 mTorr pressure, 40 W RF

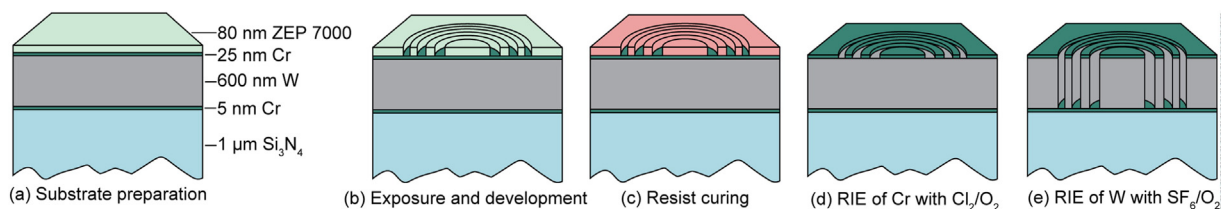


Fig. 1. Fabrication process of tungsten zone plates. (a) Substrate preparation. (b) The zone plate pattern is written using electron beam lithography and then developed. (c) The remaining resist is cured with a large electron dose. (d) Using reactive ion etching, the pattern is transferred into chromium. (e) The pattern is finally etched into tungsten.

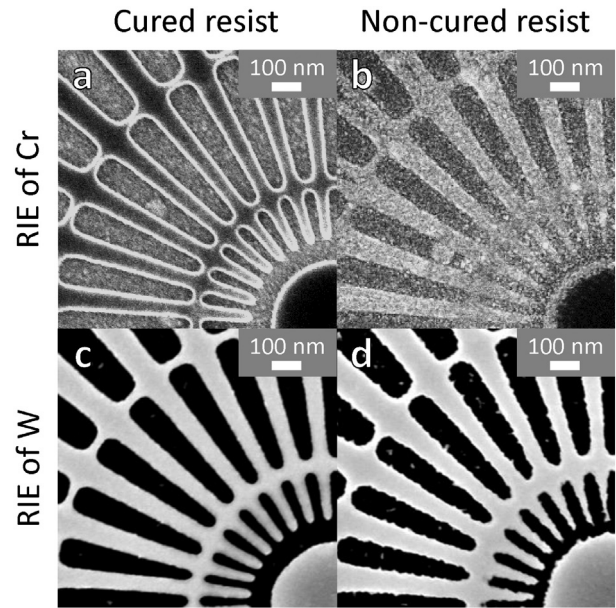


Fig. 2. Comparison of pattern transfer quality in test samples using cured and non-cured resists. Top view of hardmask after pattern transfer into the hardmask layer (a) with curing, (b) without curing; after pattern transfer into tungsten (c) with curing, (d) without curing.

power, 50 W ICP power,  $-35$   $^{\circ}\text{C}$  substrate temperature, resulting in an etch rate of around 50 nm/min. Sidewall angles are controlled by etching at cryogenic temperatures [15], as well as low process gas pressure. The final zone plate has a diameter of 200  $\mu\text{m}$ , outermost zone width of 30 nm, and a first order focal length of 40 mm at 8.2 keV photon energy.

### 2.2. Characterization

The zone plate performance was quantified in a synchrotron environment at the coherence beamline (I13-1) at the Diamond Light Source [16]. The measurement details are described in this section.

For the experiments, several zone plates of approximately 600 nm thickness were used. They were illuminated by a coherent beam with 8.2 keV photon energy. A 500  $\mu\text{m}$  aperture with a 25  $\mu\text{m}$ -wide, 25  $\mu\text{m}$ -thick tungsten central stop was placed directly behind a zone plate, while a 10  $\mu\text{m}$  pinhole was placed slightly upstream of the focal plane of the optic. This configuration suppressed 0th order illumination and blocked higher diffraction orders so that only the 1st order is recorded by a scintillator-based high resolution X-ray camera.

## 3. Results

Images of zone plates fabricated using the process described in this paper are presented in this section. The main limiting factor in this study was identified to be the fabrication of structures with a straight vertical profile. The underlying causes and consequences are discussed.

To begin with, the vertical profiles of a finished zone plate are depicted in Fig. 3. It must be noted that these structures were designed to terminate, and as such they are not truly a cross-section of a zone plate. Even though the etching process is highly anisotropic, diffusion is enhanced at the open ends of the trenches where etch rate is then increased.

After reactive ion etching of the chromium hardmask there is still some resist left if it is cured (dark areas with white outlines in Fig. 2a). Conversely, under identical process parameters the resist is completely etched away if it is left uncured and only the hardmask material is visible (light areas in Fig. 2b). Consequently, it can be clearly observed that the line-edge roughness of the mask is reduced (Fig. 2c), compared to skipping the curing step (Fig. 2d). In addition, patterned structures down to 30 nm are fully intact in the mask. The increased pattern transfer fidelity results in smooth vertical walls in the final zone plate structure.

However, it was difficult to maintain vertical sidewall profiles in dense patterns. As shown in Fig. 3a and 3b, the sidewalls are slightly slanted at the bottom and also experience minor bowing throughout. Attempts at line width reduction to 25 nm led to structural collapse of tungsten, attributed to this bowing.

Hypothetically, the phenomenon could be alleviated by reducing the gas pressure during the etching process. However, during fabrication trials it proved to be challenging to maintain plasma at pressures lower than 4 mTorr. Preferably an alternate set of reactive ion etching parameters should be researched for further development of the process. For example, decreasing substrate temperature during the final etch step while simultaneously increasing the power of the radio frequency electromagnetic field or the inductively coupled plasma.

Finally, the theoretical efficiency of a 630 nm-thick device with identical parameters at 8.2 keV is 11.3%. However, the best result of total zone plate efficiency was 2.2%. The lower measured efficiency in the fabricated real zone plate can be explained by the imperfect zone shapes in the optic as well as a lower density of the sputtered film compared to solid tungsten.

This fact is confirmed as shown in Fig. 4 which depicts local zone plate efficiency at 8.2 keV. It can be observed that the efficiency decreases towards the edge of the zone plate. This indicates that the overall decreased performance is indeed partly due to flaws in the vertical zone profile. The concentric artifacts that can be seen in the

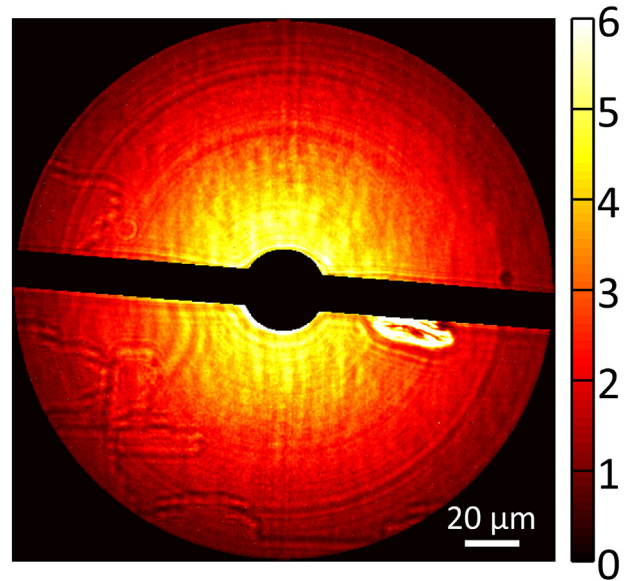


Fig. 4. Local zone plate efficiency in percent.

image can be attributed to fabrication faults, whereas other streaks are caused by debris on the elements in the optical path.

#### 4. Conclusion

In this paper, we presented an improved way to fabricate high aspect ratio tungsten nanostructures. Including a resist curing step into the existing process increases the fidelity of pattern transfer. We show and characterize a Fresnel zone plate manufactured using this recipe. The optic has a 30 nm outermost zone width and 630 nm zone height, and thus an aspect ratio of 21:1. A lower than expected total efficiency of 2.2% is attributed to the imperfect vertical profile of the outermost zones and diminished density of sputtered tungsten. This is also identified as the limiting factor in the current process. We suggest a possible improvement by reducing etching process pressure, but encourage parameter space exploration for alternative routes.

Even though presently there are superior techniques available for the purpose of X-ray diffractive optics, this study is an important improvement for nanopatterning of tungsten. The process is very versatile and can be used for other applications, such as high-resolution X-ray test samples and contact masks for X-ray lithography.

#### Acknowledgments

We thank Ulrich Wagner and Christoph Rau for their help with the experiments at the Diamond Light Source beamline I-13-1.

A portion of this work was carried out with the support of the Diamond Light Source. We thank Diamond Light Source for access to beamline I-13-1 (proposal number MT12046) that contributed to the results presented in this paper.

We gratefully acknowledge financial support from the Swedish Research Council (grant ID C0242401) and the Knut and Alice Wallenberg Foundation.

#### References

- [1] A. Sakdinawat, D. Attwood, *Nat. Photonics* 4 (2010) 840–848.
- [2] P.F. Tavares, S.C. Leemann, M. Sjöström, A. Andersson, J. Synchrotron. Radiat. 21 (2014) 862–877.
- [3] D. Attwood, *Soft X-rays and Extreme Ultraviolet Radiation: Principles and Applications*, Cambridge University Press, Cambridge, 1999.
- [4] J. Reinspach, F. Uhlén, H.M. Hertz, A. Holmberg, *J. Sci. Technol. B* (2011) 06FG02.
- [5] F. Uhlén, D. Nilsson, J. Rahomäki, L. Belova, C.G. Schroer, F. Seiboth, A. Holmberg, H.M. Hertz, U. Vogt, *Microelectron. Eng.* 116 (2014) 40–43.

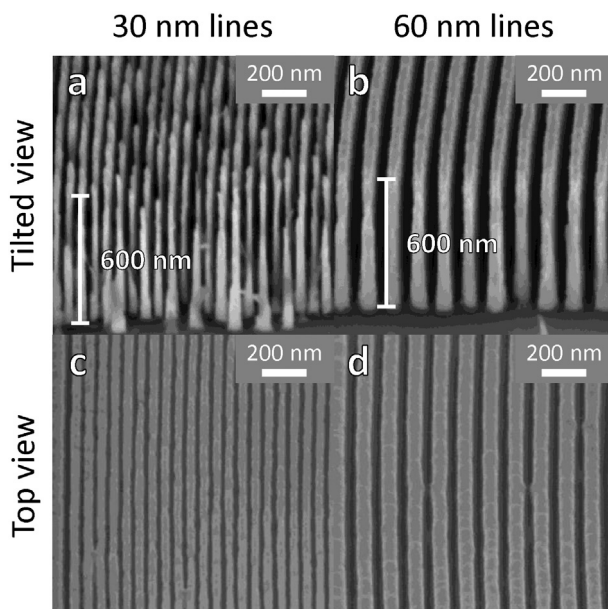


Fig. 3. Vertical zone profile with line width of (a) 30 nm and (b) 60 nm. Top view of the zone plate structures at line width of (c) 30 nm, (d) 60 nm.

- [6] C. Chang, A. Sakdinawat, *Nat. Commun.* 5 (2014).
- [7] J. Vila-Comamala, S. Gorelick, E. Färm, C.M. Kewish, A. Diaz, R. Barrett, V. Guzenko, M. Ritala, C. David, *Opt. Express* 19 (2011) 175–184.
- [8] J. Vila-Comamala, K. Jefimovs, J. Raabe, T. Pilvi, R.H. Fink, M. Senoner, A. Maassdorf, M. Ritala, C. David, *Ultramicroscopy* 109 (2009) 1360–1364.
- [9] I. Mohacsi, I. Vartiainen, M. Guizar-Sicairos, P. Karvinen, V.A. Guzenko, E. Müller, E. Färm, M. Ritala, C.M. Kewish, A. Somogyi, C. David, *Opt. Express* 23 (2015) 776.
- [10] A.J. Morgan, M. Prasciolu, A. Andrejczuk, J. Krzywinski, A. Meents, D. Pennicard, H. Graafsma, A. Barty, R.J. Bean, M. Barthelmess, D. Oberthuer, O. Yefanov, A. Aquila, H.N. Chapman, *Sci. Report.* 5 (2015) 9892.
- [11] P. Charalambous, *AIP Conf. Proc.* 507 (2000) 625–630.
- [12] J. Reinspach, M. Lindblom, O. von Hofsten, M. Bertilson, H.M. Hertz, A. Holmberg, *J. Vac. Sci. Technol. B* 27 (2009) 2593.
- [13] T. Oyama, H. Nakamura, *Appl. Phys. Ex.* 7 (2014) 035601.
- [14] D.A. Czaplewski, L.E. Ocola, *J. Vac. Sci. Technol. B* 29 (2011) 021601.
- [15] Z. Liu, Y. Wu, B. Harteneck, D.L. Olynick, *Nanotechnology* 24 (2013) 015305.
- [16] C. Rau, U. Wagner, Z. Pešić, A. De Fanis, *Phys. Status Solidi Appl. Mater. Sci.* 208 (2011) 2522–2525.